AGU ADVANCING EARTH AND SPACE SCIENCES

Geophysical Research Letters®

Key Points:

- The solar forcing pattern effect is investigated in a coupled ocean-atmosphere model
- Climate sensitivity is doubled from tropical forcing to Southern Ocean forcing
- The radiative forcing pattern effect involves changes in lapse rate feedback, cloud feedback, and tropospheric stability

Supporting Information:

Supporting Information may be found in the online version of this article.

Correspondence to:

B. Zhang,
bosongzhang@gmail.com

The Dependence of Climate Sensitivity on the Meridional Distribution of Radiative Forcing

Bosong Zhang[1] , Ming Zhao[2] , Haozhe He[3] , Brian J. Soden[3] , Zhihong Tan[1] , Baoqiang Xiang[2] , and Chenggong Wang[1]

[1]Program in Atmospheric and Oceanic Sciences, Princeton University, Princeton, NJ, USA, [2]NOAA/Geophysical Fluid Dynamics Laboratory, Princeton, NJ, USA, [3]Rosenstiel School of Marine, Atmospheric and Earth Science, University of Miami, Miami, FL, USA

Abstract This study investigates how climate sensitivity depends upon the spatial pattern of radiative forcing. Sensitivity experiments using a coupled ocean-atmosphere model were conducted by adding anomalous incoming solar radiation over the entire globe, Northern Hemisphere mid-latitudes, Southern Ocean, and tropics. The varied forcing patterns led to highly divergent climate sensitivities. Specifically, the climate is nearly twice as sensitive to Southern Ocean forcing as tropical forcing. Strong coupling between the surface and free troposphere in the tropics increases the inversion strength, leading to smaller cloud feedback in the tropical forcing experiments. In contrast, the extratropics exhibit weaker coupling, a decrease or near-zero change in the inversion strength, and strong positive cloud feedback. These results contrast with the conventional SST-pattern effect in which tropical surface temperature changes regulate climate sensitivity. They also have important implications for other potentially asymmetric forcings, such as those from geoengineering, volcanic eruptions, and paleoclimatic changes.

Plain Language Summary The way surface temperature responds to radiative forcing depends on where such forcing is applied. Numerical model integrations show that the global mean surface temperature change is doubled when the forcing is imposed over the Southern Ocean compared to when the forcing is applied in the tropics. Changes in the vertical temperature profiles and clouds contribute to the dependence of surface temperature change on the forcing geographic locations.

1. Introduction

A linear zero-dimensional energy balance model is a useful tool for understanding the relationship between radiative forcing and surface temperature. It provides a straightforward way to estimate climate sensitivity (Gregory et al., 2004). However, this framework does not account for the spatial pattern of surface temperature changes. Specifically, the spatial pattern of sea surface temperature (SST) change has received much attention. Previous studies have shown that the spatial pattern of SST has great impacts on precipitation (Xie et al., 2010), large-scale circulation (Ma & Xie, 2013), the global radiative budget and thus radiative feedbacks (Andrews & Webb, 2018; Andrews et al., 2022). In particular, the dependence of radiative feedbacks on SST spatial patterns is of great interest to the community (Andrews & Webb, 2018; Andrews et al., 2015), as model feedback and predicted climate sensitivity can vary considerably between different patterns of SST changes even though these patterns have the same global mean values (Zhao, 2022). To estimate the impacts of SST spatial patterns on climate feedback and sensitivity, recent studies have utilized a Green's function approach to analyze the climate response to local SST changes in atmosphere-only models forced by monthly varying SST, and have shown that SST warming over tropical warm pools is associated with strong global-mean radiative cooling, whereas the same amount of SST warming over mid-to-high latitudes (e.g., the Southern Ocean) induces relatively small global-mean radiative response (Dong et al., 2019; Zhang et al., 2023; Zhou et al., 2017).

While the Green's function approach has shown to be useful in understanding the SST pattern effect on radiative feedback and climate sensitivity, large uncertainties exist in terms of future SST projections. It is important to understand the radiative forcing pattern effect in ocean-atmosphere coupled models, where SST response to radiative forcing can be retrieved from such models. Motivated by the SST pattern effect on radiative feedbacks, this study seeks to explore how spatial asymmetries in radiative forcing influence climate sensitivity through a series of idealized solar forcing experiments using an ocean-atmosphere coupled system, which can help us understand

paleoclimate and guide the development of potential geoengineering like climate intervention strategies in the future.

Previous studies have examined impacts of forcing patterns on the climate system from different perspectives. For example, Stuecker et al. (2020) showed that both local and remote CO_2 forcing affect equatorial temperature via the large-scale atmospheric circulation like the Hadley cell, the oceanic circulation, and local cloud feedback. Compared with tropical forcings, extratropical forcings have a greater impact on global temperature change (de F. Forster et al., 2000; Joshi et al., 2003). Similarly, ocean heat uptake in higher latitudes results in greater global surface temperature change than ocean heat uptake in lower latitudes, which is attributed to distinct cloud feedbacks and circulation changes (Kang & Xie, 2014; Liu et al., 2018; Rose et al., 2014; Rugenstein et al., 2016). Extratropical radiative forcings also shift the position of the intertropical convergence zone by modifying the meridional energy transport (Kang et al., 2019; Xiang et al., 2018).

Quantifying radiative forcing pattern effect not only helps understanding of paleoclimate but also provides insight for future climate intervention strategies. For example, previous studies have shown that variations in obliquity alter the meridional distribution of incoming solar radiation at TOA, which further affects SST and climate feedbacks (Mantsis et al., 2011), and large-scale circulation (Mantsis et al., 2014). Orbital precession can also change the energy budget at TOA, which impacts the Hadley cell (Merlis et al., 2013a, 2013b) and tropical precipitation (Merlis et al., 2013c). In terms of potential climate intervention strategies, injecting aerosol into the stratosphere emerges as one of the feasible approaches that alters the energy balance of the climate system (Irvine et al., 2016). The increased aerosol in the stratosphere modifies radiative forcing pattern, indicating a tight connection between radiative forcing pattern effect and climate intervention strategies.

In this study, we investigate the dependence of climate feedback and sensitivity on the spatial pattern of solar forcing in a coupled climate model. Specifically, the incoming solar radiation at TOA is perturbed at different geographic locations to mimic the effect of changes in the spatial pattern of radiative forcing. A series of perturbation experiments are conducted by imposing an abrupt change of incoming solar radiation over the entire globe, and three zonal bands including the Northern Hemisphere mid-latitudes, Southern Ocean, and tropics. These experiments reveal a strong dependence of climate sensitivity upon the spatial pattern of radiative forcing, with extratropical forcings inducing roughly twice as much global-mean temperature change as tropical forcings, particularly in the Southern Hemisphere. The global mean temperature dependence on forcing locations is primarily contributed by synchronous changes in lapse rate and tropospheric stability, and their combined effect on low cloud feedback.

2. Methods

2.1. Idealized Spatial Patterns of Solar Forcing Perturbation

Applying a fractional change to the solar constant is one approach of modifying incoming solar radiation. However, since the amplitude of annual mean incoming solar radiation peaks at the equator and decreases poleward, the resulting solar perturbation by this approach varies with latitude. This makes it challenging to determine whether the response is due to the amount of the fractional change, the spatial pattern of the perturbation, or a combination of both. The goal is to investigate the dependence of climate response on the location of anomalous incoming solar radiation. To achieve this, we impose solar forcing perturbation over the entire globe, Northern Hemisphere Mid-latitudes, Southern Ocean, and Tropics. We seek to ensure that the annual mean anomalies are horizontally uniform, thereby excluding any potential impacts from the heterogeneity of imposed forcing within the regions of interest. By doing so, we can better understand the dependence of climate response on the location of the forcing and its potential implications for climate sensitivity.

The annual mean distribution of incoming solar radiation for the Earth can be sufficiently approximated by:

$$\hat{\sigma}_2(y) = 1 - 0.482 \times p_2(y) \tag{1}$$

where y stands for sine of latitude and $p_2(y)$ is the second-order Legendre polynomial with $p_2(y) = (3y^2 - 1)/2$ (Nadeau & McGehee, 2017; North, 1975). In this form, the annual mean distribution of incoming solar radiation is only a function of latitude. At each model time step, the incoming solar radiation perturbation is deduced by normalizing the model-computed solar flux by Equation 1, and then multiplying the normalized term with a

parameter to modify the magnitude of the perturbation. By doing this, only the annual mean perturbation is horizontally uniform, whereas neither the instantaneous nor the monthly mean perturbation is.

In this study, we consider both positive and negative perturbations. To ensure that the experiments are comparable with each other for the same sign, we keep the absolute magnitude of the global mean forcing the same. Since the domain size varies across the experiments, the parameter used to control the magnitude depends on the domain size. Specifically, positive perturbation experiments have a global mean forcing of +4 Wm^{-2} while the negative ones have a global mean forcing of −4 Wm^{-2}. The geographic locations of anomalous incoming solar radiation are shown in Figure S1 in Supporting Information S1. Note that neither global mean effective radiative forcing nor global mean instantaneous radiative forcing is supposed to be the same across all experiments by this approach.

2.2. Model and Experiment

The Seamless System for Prediction and EArth System Research, developed at NOAA's Geophysical Fluid Dynamics Laboratory (GFDL), is a fully coupled model designed for physical climate prediction and projection over a range of timescales from seasonal to multidecadal (Delworth et al., 2020). In this study, the SPEAR_LO version is used, which consists of AM4 for the atmosphere component and LM4 for the land component (Zhao et al., 2018a, 2018b). The atmosphere model has 33 vertical levels with a horizontal resolution of approximately 100 km. The ocean and sea ice components are based on the MOM6 model and have a nominal horizontal resolution of 1° and 75 vertical levels. Further information on the SPEAR_LO can be found in Delworth et al. (2020).

In this study, a preindustrial control simulation integrated for 400 years is used as a base state, with radiative gas concentration and aerosol emission fixed at levels representative of the calendar year 1850. As noted in Delworth et al. (2020), this simulation displays a radiative imbalance at the TOA close to zero and little change in global mean surface air temperature over the 400-year period, indicating that the system is in near equilibrium. The climatological mean state is calculated from model outputs between years 101 and 300. For the perturbed simulations, initial conditions are retrieved from year 101 of the Control simulation, and an abrupt anomalous incoming solar radiation is added and maintained at a constant level throughout each simulation. The domain of interest for each experiment is listed in Table S1 in Supporting Information S1. Each perturbed simulation is integrated for 200 years.

2.3. Radiative Kernel Analyses

The radiative kernels used in this study are based on the atmospheric component of a recent generation climate model (HadGEM3) developed by the UK Met Office (Smith et al., 2020). The radiative kernel method decomposes the response of radiative fluxes at the TOA into individual components caused by changes in temperature, water vapor, surface albedo and clouds. Soden et al. (2008) showed that cloud feedback can be diagnosed from the response of cloud radiative effect corrected by cloud masking effect. The radiative kernel method quantifies radiative responses from changes in Planck (contributions of vertically uniform warming), lapse rate (contributions of departures from vertically uniform warming), water vapor, surface albedo, and cloudiness. Here we compute radiative feedbacks as the difference between Control climatology and the last 20 years of the perturbation experiments. Note that using the last 50 years of the perturbation experiments yields similar results.

3. Surface Temperature Response and Climate Sensitivity

Figure 1 illustrates impacts of anomalous incoming solar radiation on surface temperature changes. Here the negative of the surface temperature responses are shown for the negative forcing experiments. The globally uniform positive forcing, GL +4, results in an overall surface warming except in the North Atlantic high latitudes (Figure 1a). NM +4 leads to enhanced surface warming over the Northern Hemisphere continents and the North Pacific, whereas the North Atlantic high latitudes still exhibit anomalous surface cooling (Figure 1b). By contrast, SO +4 shows large surface warming not only over the entire Southern Ocean but also over the tropical eastern Pacific and tropical Atlantic, although with a weaker warming hole over the North Atlantic (Figure 1c). The teleconnection between the SO and the tropics involves several proposed mechanisms such as low cloud feedbacks (Kim et al., 2022; Zhang et al., 2021) and surface wind anomalies associated with the Antarctic ozone
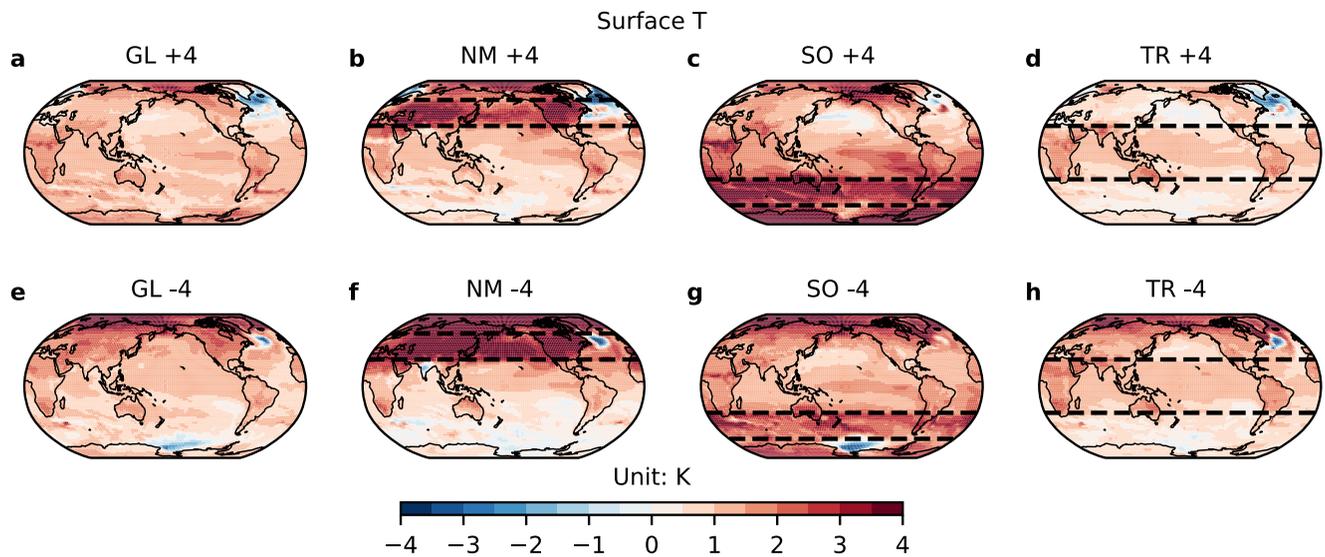
Figure 1. Maps of surface temperature changes (i.e., sea surface temperature over ocean and surface skin temperature over land; units: K) averaged over the last 50 years (year 151–200) of each simulation relative to the base state of Control. The dashed lines in NM, SO, and TR mark the geographical boundaries of the anomalous solar forcing imposed. The negative of the surface temperature responses are shown for the negative forcing experiments (e–h).

hole (Hartmann, 2022). TR +4 exhibits a similar surface warming pattern as GL +4, but with a weaker magnitude (Figure 1d). The negative perturbation experiments show similar patterns of surface temperature changes as their positive counterparts, although the responses are not fully symmetric (Figures 1e–1h).

The distinctive SST responses over the North Atlantic high latitudes indicate changes in the Atlantic Meridional Overturning Circulation (AMOC), which is tightly connected with the SST changes over the North Atlantic (Zhang & Delworth, 2005). Previous modeling studies reported a reduction in AMOC strength as the climate warms, which is due to an increase in local surface heat fluxes and surface freshwater fluxes, although their relative importance varies (Gregory et al., 2005; Weaver et al., 2007). A weakened AMOC is found to cause a cooling tendency to the south of Greenland in the North Atlantic (Liu et al., 2020). Here we find that NM +4 has the most reduction in the AMOC strength while NM −4 has the most increase (Figure S2 in Supporting Information S1), which is consistent with the anomalous North Atlantic SST in NM cases as shown in Figure 1. While similar AMOC responses are found in GL and TR cases, AMOC is hardly affected in SO cases (Figure S2 in Supporting Information S1), indicating that forcing over the Southern Hemisphere mid-latitude may not alter transient AMOC strength very much, although possible changes may appear with longer integration. Within the 200-year simulation, it is the forcing in the Northern Hemisphere mid-latitude that greatly changes the AMOC strength.

Overall, the varied patterns of surface temperature responses in Figure 1 indicate variations in climate sensitivity. Near the end of the simulations, the global mean temperature change in SO cases is nearly twice as large as that in TR cases (Figure S3 in Supporting Information S1). Although the global mean responses are not exactly symmetric between the positive and negative forcing experiments, the dependence of climate sensitivity on the geographic locations of the imposed anomalous incoming solar radiation indicates robust *radiative forcing pattern effect*. However, the radiative forcing pattern effect may be model dependent and thus require more modeling evidence in the future to strengthen the findings shown in this study. On the other hand, using simple energy balance models may shed more light on the radiative forcing pattern effect. For example, Lutsko et al. (2020) found that in addition to the latitudinal profiles of insolation reduction, the effectiveness of reducing incoming solar radiation exhibits state dependence. The state dependence is beyond the scope of this study and can be explored in the future.

Previously Winton et al. (2010) introduced the ocean heat uptake efficacy factor (definition can be found in Section 3 in Winton et al. (2010)) to address climate response to an increase in CO_2 concentration. The efficacy factor was explained in the context of a two-box model by Held et al. (2010), and was used to account for the effect of evolving SST spatial patterns on climate feedback (Winton et al., 2020). Here, large values of ε are mainly found in TR (not shown), indicating strong damping of the imposed forcing and thus large negative radiative
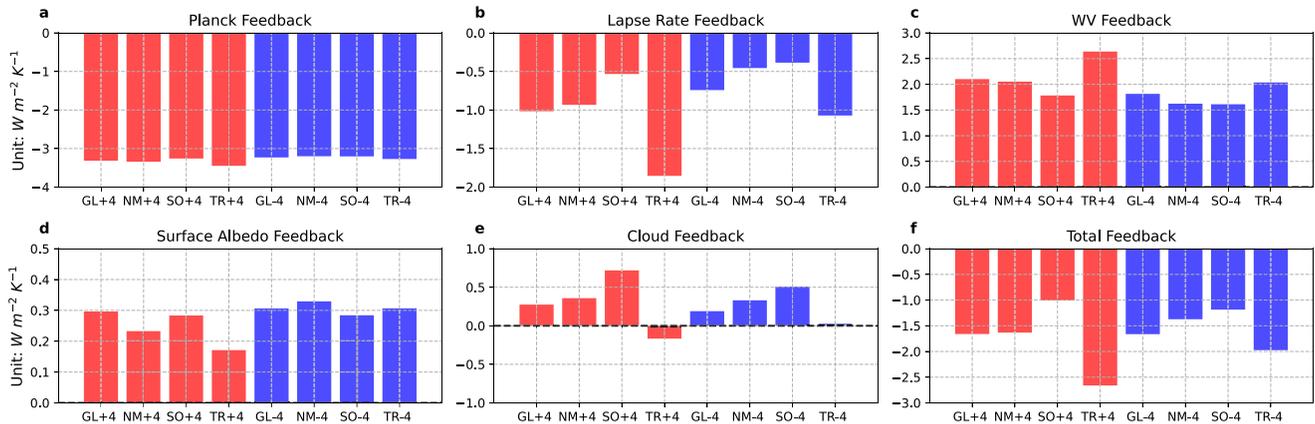
Figure 2. The global mean (a) Planck feedback, (b) lapse rate feedback, (c) water vapor feedback, (d) surface albedo feedback, (e) cloud feedback, and (f) total radiative feedback (units: W m⁻² K⁻¹). Positive forcing experiments are in red while negative forcing experiments are in blue.

feedback, whereas small values of ε mostly appear in extratropical forcing cases (NM and SO) and global forcing cases (GL), which suggests weak damping of the imposed forcing and thus small negative radiative feedback. In addition, as indicated by the time series of global mean surface air temperature (Figure S3 in Supporting Information S1), the negative perturbation experiments evolve toward equilibrium in a faster pace than the positive ones. Stouffer (2004) showed that the coupled system exhibits a shorter response time scale with an abrupt half of CO_2 concentration than an abrupt doubling of CO_2 concentration. Variations of the response times scale between positive and negative forcing suggest that one may not use the relationship found solely from either positive forcing or negative forcing experiments to constrain transient climate sensitivity (Merlis et al., 2014).

4. Radiative Feedbacks

To understand solar forcing pattern effect, we diagnose radiative feedbacks using the radiative kernel method (see Section 2). The Planck feedback is negative and shows relatively small variations across the perturbation experiments (Figure 2a). The lapse rate feedback is also negative but exhibits larger variations (Figure 2b) primarily due to differences in the surface warming patterns caused by changes in solar forcing location. The coupling between the surface and the free troposphere is strongest in the tropics, where the temperature response closely follows a moist adiabat. Therefore, a relatively larger warming in the tropics is associated with more tropospheric warming, a greater reduction in lapse rate, and a more negative lapse rate feedback (Soden & Held, 2006). The tropical forcing has more warming at low latitudes and therefore greater free tropospheric warming per unit global surface temperature change (Figure S4 in Supporting Information S1). In contrast, the extratropical forcing, especially for the SO, has more surface warming at high latitudes where the surface-troposphere coupling is weak, which leads to less free tropospheric warming, a smaller change in lower tropospheric stability, and a less negative lapse rate feedback (Figure 2b). This difference in the vertical structure of free tropospheric warming is clearly evident in the vertical profiles of global-mean air temperature change (Figure S4 in Supporting Information S1).

Understanding the radiative forcing pattern effect on lapse rate feedback is important for estimation of climate sensitivity given that it is hard to constrain lapse rate feedback based on observations (He et al., 2021). Additionally, we note the positive forcing experiments tend to have a larger lapse rate feedback than the negative forcing experiments, which is mainly due to the increased moisture content as the climate warms. More water vapor means an increase in latent heat release as parcels rise, which leads to a steeper moist adiabatic lapse rate (Held & Soden, 2000). Indeed, the water vapor feedback is larger in the positive forcing experiments than that in the negative forcing experiments (Figure 2c). An in-depth review of water vapor feedback and lapse rate feedbacks can be found in Colman and Soden (2021). Lastly, the surface albedo feedback is also positive but is relatively small in magnitude (Figure 2d).

Not surprisingly, the range in cloud feedback is large between these experiments (Figure 2e). The cloud feedback in TR +4 is slightly negative and becomes almost zero in TR −4. By contrast, large positive cloud feedback is found in SO cases. Overall, the large spread in lapse rate feedback and cloud feedback contributes to the spread
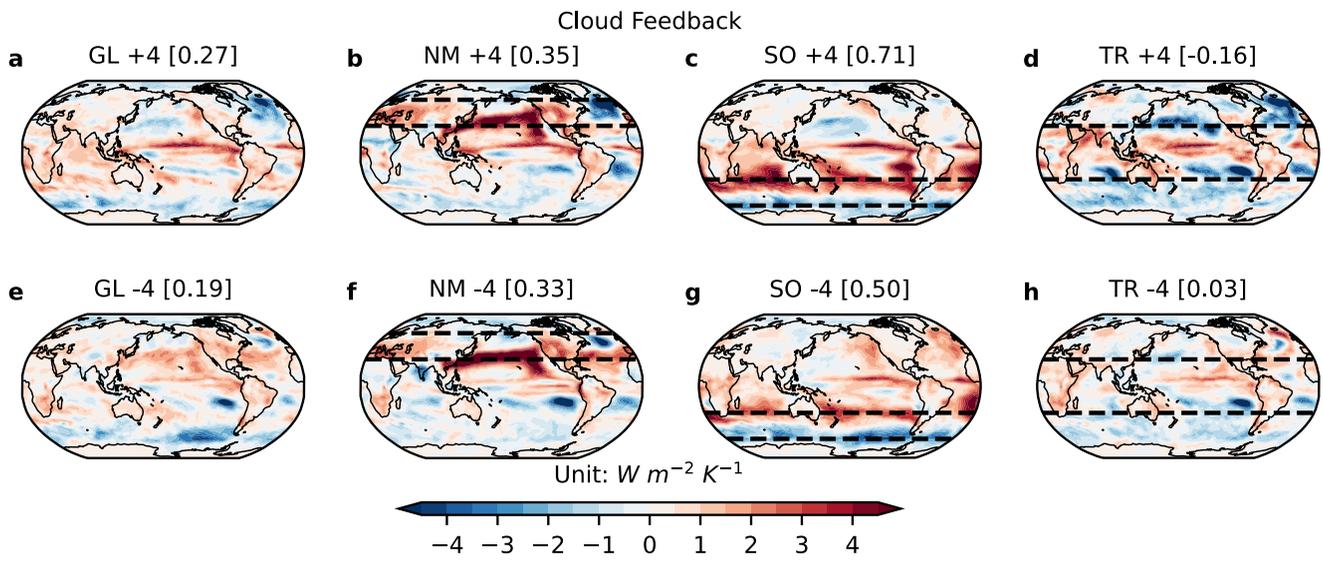
Figure 3. Maps of local cloud feedback (units: W m^{-2} K^{-1}). The global mean values are listed in the square brackets.

in total radiative feedback, where TR +4 is roughly -2.5 W m^{-2} K^{-1} but SO +4 is roughly -1.0 W m^{-2} K^{-1} (Figure 2f).

Maps of local cloud feedback (i.e., cloud induced radiative perturbations at TOA corrected by cloud masking effect and then divided by global mean surface air temperature change) are shown in Figure 3. For TR cases, negative values in the extratropics and positive values in the deep tropics tend to offset, leading to slightly negative global mean cloud feedback in TR +4 (Figure 3d) and nearly zero one in TR -4 (Figure 3h). For SO cases, positive values are found mostly over tropical and subtropical oceans, especially over the stratocumulus-dominated areas such as the Southeast Pacific and Atlantic (Figures 3c and 3g). Recently, Kang et al. (2023) showed that surface warming over the Southern Ocean yields a strong positive cloud feedback, especially over the southeast Pacific. Overall, our results are consistent with those in Kang et al. (2023). In terms of NM cases, positive values mainly appear over the north Pacific (Figures 3b and 3f). Such patterns yield an overall more positive global mean cloud feedback.

5. Connection to Cloud Controlling Factors

Then the question is: why do changes in the forcing location alter the sign and magnitude of cloud feedback? Recent studies proposed that meteorological cloud-controlling factors like SST and estimated inversion strength (EIS) (Wood & Bretherton, 2006) among other variables can explain changes in cloud amount and thus cloud feedback, especially low cloud feedback (Myers et al., 2021; Scott et al., 2020). Among the proposed cloud-controlling factors, we find that EIS is a primary factor affecting the cloud feedback, while other factors like mid-level specific humidify and vertical velocity show no robust relationship with the cloud feedback. Here, changes in EIS are normalized by global mean surface temperature changes (Figure 4) to allow for a direct comparison with the cloud feedback. Large positive values are found in TR cases, indicating a more stable troposphere in a warmer climate that favors more low cloud amount, and results in enhanced radiative cooling and negative cloud feedback in the tropics and subtropics (Figures 3d and 3h). In comparison, the EIS response in NM and SO cases show interhemispheric asymmetry. Negative values are mostly found in the forcing domain, which indicates locally decreased stability in a warmer climate. As a result, positive cloud feedback becomes dominant and contributes to the overall positive global mean cloud feedback in NM and SO cases.

The changes in EIS covary with the changes in lapse rate feedback. A more negative lapse rate feedback means relatively more tropospheric warming than surface warming, which tends to enhance the tropospheric stability (Figure 5a). The increased tropospheric stability favors more cloud cover and thus leads to a more negative cloud feedback (Figure 5b). In addition, the positive forcing experiments tend to have a larger lapse rate and EIS response than the negative forcing experiments because of the moist adiabat dependence on temperature.
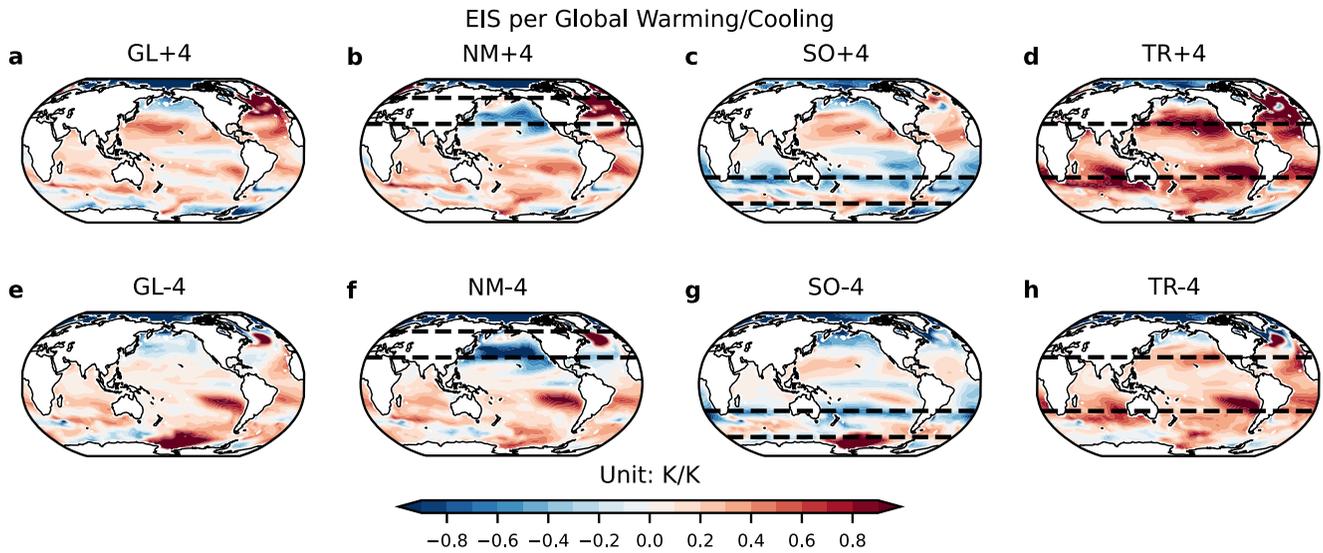
Figure 4. Maps of changes in estimated inversion strength per degree of global mean temperature change (units: K K^{-1}).

6. Discussions and Summary

This study investigates how changes in locations of imposed solar forcing affect the climate system in an ocean-atmosphere coupled model. We conduct a series of sensitivity experiments where anomalous incoming solar radiation is imposed globally and over three zonal bands including the Northern Hemisphere mid-latitudes, Southern Ocean, and tropics. Our analyses show that extratropical forcing results in larger temperature change compared to tropical forcing. The range in climate sensitivity mainly stems from variations in lapse rate feedback and cloud feedback, in which both are related to changes in tropospheric stability.

Our results have implications for historical aerosol forcing, volcanic eruptions, and potential climate intervention efforts in the future. Compared to the idealized solar forcing experiments, aerosol forcing involves larger spatial-temporal variability. Over the historical period, changes in anthropogenic aerosols play an important role in altering radiative forcing, which is mostly due to a geographic shift of major aerosol emission sources. The spatial distribution of aerosols impacts surface temperature responses (Persad & Caldeira, 2018; Xiang
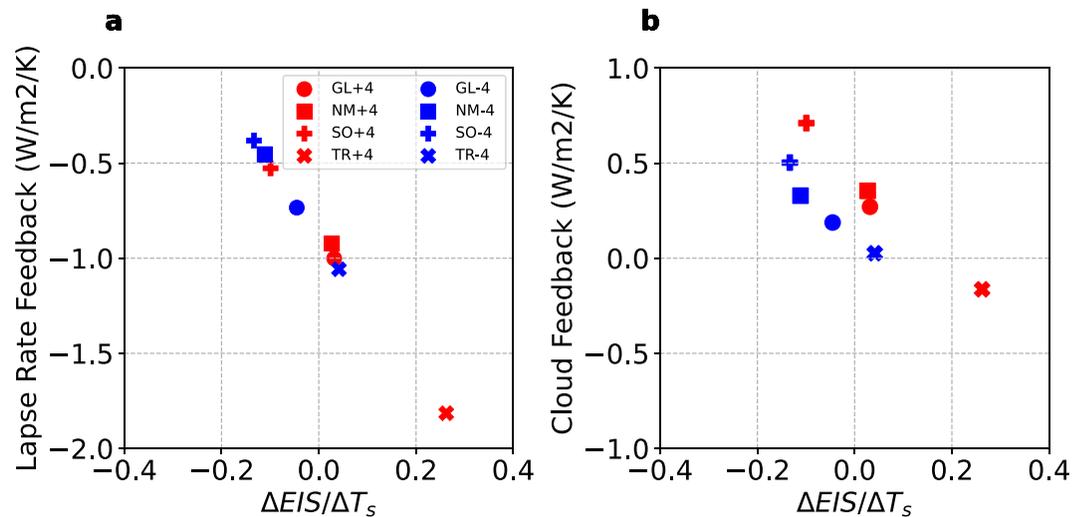

Figure 5. Scatterplots of (a) changes in global mean estimated inversion strength (EIS) per degree of global mean temperature change (units: K K^{-1}) versus lapse rate feedback, and (b) changes in EIS per degree of global mean temperature change (units: K K^{-1}) versus cloud feedback.

et al., 2023). Potential climate intervention approaches such as injecting sulfate into the stratosphere also exhibits latitudinal dependence where extratropical injection is more efficient in reducing global temperature (MacMartin & Kravitz, 2019; Tilmes et al., 2017). However, such aerosol injection is not equivalent to directly reducing incoming solar radiation. Anomalous stratospheric aerosols can induce circulation changes (Visioni et al., 2021). Therefore, caution should be taken care of when comparing the idealized solar forcing experiments with the actual climate intervention strategies like stratospheric aerosol injection. In addition, volcanic eruptions can also induce an abrupt change in the geographic distribution of aerosols, which can further affect the mean state of the climate system (Yang et al., 2019). As indicated by the simulations, zonally symmetric forcing in the extratropics induces larger global mean temperature changes than that in the tropics. This implies that the effectiveness of geoengineering in modifying the overall mean state of the climate system would be limited if the forcing is applied solely over the tropics. Alternatively, our results highlight the importance of carefully choosing the location of the forcing when developing and evaluating potential climate intervention strategies.

Overall, the results in this study provide evidence of the solar forcing pattern effect on the climate system, which involves dependence of radiative feedbacks on the geographic locations of solar forcing. Considering the computational cost of running coupled climate models, we only apply zonally symmetric forcing over the entire globe and three individual zonal bands, and perturb the entire shortwave spectrum of the solar radiation. We acknowledge that the solar forcing's spatial pattern can be more complex. Also, the perturbation is applied to the entire spectrum of solar radiation. A recent study suggested that the impact of solar radiation is spectrally dependent (Jing et al., 2021). While these issues are beyond the scope of this study, we suggest that future research could explore related questions, building on our findings to gain a more comprehensive understanding of the multifaceted interactions between external radiative forcing, feedback, surface temperature, and other aspects of the climate system.

Data Availability Statement

The data can be found at Zenodo (https://zenodo.org/record/8302960).

References

Andrews, T., Bodas-Salcedo, A., Gregory, J. M., Dong, Y., Armour, K. C., Paynter, D., et al. (2022). On the effect of historical SST patterns on radiative feedback. *Journal of Geophysical Research: Atmospheres*, *127*(18), e2022JD036675. https://doi.org/10.1029/2022jd036675

Andrews, T., Gregory, J. M., & Webb, M. J. (2015). The dependence of radiative forcing and feedback on evolving patterns of surface temperature change in climate models. *Journal of Climate*, *28*(4), 1630–1648. https://doi.org/10.1175/jcli-d-14-00545.1

Andrews, T., & Webb, M. J. (2018). The dependence of global cloud and lapse rate feedbacks on the spatial structure of tropical Pacific warming. *Journal of Climate*, *31*(2), 641–654. https://doi.org/10.1175/jcli-d-17-0087.1

Colman, R., & Soden, B. J. (2021). Water vapor and lapse rate feedbacks in the climate system. *Reviews of Modern Physics*, *93*(4), 045002. https://doi.org/10.1103/revmodphys.93.045002

de F. Forster, P., Blackburn, M., Glover, R., & Shine, K. (2000). An examination of climate sensitivity for idealised climate change experiments in an intermediate general circulation model. *Climate Dynamics*, *16*(10–11), 833–849. https://doi.org/10.1007/s003820000083

Delworth, T. L., Cooke, W. F., Adcroft, A., Bushuk, M., Chen, J. H., Dunne, K. A., et al. (2020). SPEAR: The next generation GFDL modeling system for seasonal to multidecadal prediction and projection. *Journal of Advances in Modeling Earth Systems*, *12*(3), e2019MS001895. https://doi.org/10.1029/2019ms001895

Dong, Y., Proistosescu, C., Armour, K. C., & Battisti, D. S. (2019). Attributing historical and future evolution of radiative feedbacks to regional warming patterns using a Green's function approach: The preeminence of the western Pacific. *Journal of Climate*, *32*(17), 5471–5491. https://doi.org/10.1175/jcli-d-18-0843.1

Gregory, J., Dixon, K., Stouffer, R., Weaver, A., Driesschaert, E., Eby, M., et al. (2005). A model intercomparison of changes in the Atlantic thermohaline circulation in response to increasing atmospheric CO_2 concentration. *Geophysical Research Letters*, *32*(12), L12703. https://doi.org/10.1029/2005gl023209

Gregory, J., Ingram, W., Palmer, M., Jones, G., Stott, P., Thorpe, R., et al. (2004). A new method for diagnosing radiative forcing and climate sensitivity. *Geophysical Research Letters*, *31*(3), L03205. https://doi.org/10.1029/2003gl018747

Hartmann, D. L. (2022). The Antarctic ozone hole and the pattern effect on climate sensitivity. *Proceedings of the National Academy of Sciences of the United States of America*, *119*(35), e2207889119. https://doi.org/10.1073/pnas.2207889119

He, H., Kramer, R. J., & Soden, B. J. (2021). Evaluating observational constraints on intermodel spread in cloud, temperature, and humidity feedbacks. *Geophysical Research Letters*, *48*(17), e2020GL092309. https://doi.org/10.1029/2020gl092309

Held, I. M., & Soden, B. J. (2000). Water vapor feedback and global warming. *Annual Review of Energy and the Environment*, *25*(1), 441–475. https://doi.org/10.1146/annurev.energy.25.1.441

Held, I. M., Winton, M., Takahashi, K., Delworth, T., Zeng, F., & Vallis, G. K. (2010). Probing the fast and slow components of global warming by returning abruptly to preindustrial forcing. *Journal of Climate*, *23*(9), 2418–2427. https://doi.org/10.1175/2009jcli3466.1

Irvine, P. J., Kravitz, B., Lawrence, M. G., & Muri, H. (2016). An overview of the Earth system science of solar geoengineering. *Wiley Interdisciplinary Reviews: Climate Change*, *7*(6), 815–833. https://doi.org/10.1002/wcc.423

Jing, X., Huang, X., Chen, X., Wu, D. L., Pilewskie, P., Coddington, O., & Richard, E. (2021). Direct influence of solar spectral irradiance on the high-latitude surface climate. *Journal of Climate*, *34*(10), 4145–4158. https://doi.org/10.1175/jcli-d-20-0743.1

Joshi, M., Shine, K., Ponater, M., Stuber, N., Sausen, R., & Li, L. (2003). A comparison of climate response to different radiative forcings in three general circulation models: Towards an improved metric of climate change. *Climate Dynamics*, *20*(7–8), 843–854. https://doi.org/10.1007/s00382-003-0305-9

Kang, S. M., Ceppi, P., Yu, Y., & Kang, I.-S. (2023). Recent global climate feedback controlled by Southern Ocean cooling. *Nature Geoscience*, *16*(9), 1–6. https://doi.org/10.1038/s41561-023-01256-6

Kang, S. M., Hawcroft, M., Xiang, B., Hwang, Y.-T., Cazes, G., Codron, F., et al. (2019). Extratropical–tropical Interaction Model Intercomparison Project (ETIN-MIP): Protocol and initial results. *Bulletin of the American Meteorological Society*, *100*(12), 2589–2606.

Kang, S. M., & Xie, S.-P. (2014). Dependence of climate response on meridional structure of external thermal forcing. *Journal of Climate*, *27*(14), 5593–5600. https://doi.org/10.1175/jcli-d-13-00622.1

Kim, H., Kang, S. M., Kay, J. E., & Xie, S.-P. (2022). Subtropical clouds key to Southern Ocean teleconnections to the tropical Pacific. *Proceedings of the National Academy of Sciences of the United States of America*, *119*(34), e2200514119. https://doi.org/10.1073/pnas.2200514119

Liu, F., Lu, J., Garuba, O. A., Huang, Y., Leung, L. R., Harrop, B. E., & Luo, Y. (2018). Sensitivity of surface temperature to oceanic forcing via q-flux green's function experiments. Part II: Feedback decomposition and polar amplification. *Journal of Climate*, *31*(17), 6745–6761. https://doi.org/10.1175/jcli-d-18-0042.1

Liu, W., Fedorov, A. V., Xie, S.-P., & Hu, S. (2020). Climate impacts of a weakened Atlantic meridional overturning circulation in a warming climate. *Science Advances*, *6*(26), eaaz4876. https://doi.org/10.1126/sciadv.aaz4876

Lutsko, N. J., Seeley, J. T., & Keith, D. W. (2020). Estimating impacts and trade-offs in solar geoengineering scenarios with a moist energy balance model. *Geophysical Research Letters*, *47*(9), e2020GL087290. https://doi.org/10.1029/2020gl087290

Ma, J., & Xie, S.-P. (2013). Regional patterns of sea surface temperature change: A source of uncertainty in future projections of precipitation and atmospheric circulation. *Journal of Climate*, *26*(8), 2482–2501. https://doi.org/10.1175/jcli-d-12-00283.1

MacMartin, D. G., & Kravitz, B. (2019). The engineering of climate engineering. *Annual Review of Control, Robotics, and Autonomous Systems*, *2*(1), 445–467. https://doi.org/10.1146/annurev-control-053018-023725

Mantsis, D. F., Clement, A. C., Broccoli, A. J., & Erb, M. P. (2011). Climate feedbacks in response to changes in obliquity. *Journal of Climate*, *24*(11), 2830–2845. https://doi.org/10.1175/2010jcli3986.1

Mantsis, D. F., Lintner, B. R., Broccoli, A. J., Erb, M. P., Clement, A. C., & Park, H.-S. (2014). The response of large-scale circulation to obliquity-induced changes in meridional heating gradients. *Journal of Climate*, *27*(14), 5504–5516. https://doi.org/10.1175/jcli-d-13-00526.1

Merlis, T. M., Held, I. M., Stenchikov, G. L., Zeng, F., & Horowitz, L. W. (2014). Constraining transient climate sensitivity using coupled climate model simulations of volcanic eruptions. *Journal of Climate*, *27*(20), 7781–7795. https://doi.org/10.1175/jcli-d-14-00214.1

Merlis, T. M., Schneider, T., Bordoni, S., & Eisenman, I. (2013a). Hadley circulation response to orbital precession. Part I: Aquaplanets. *Journal of Climate*, *26*(3), 740–753. https://doi.org/10.1175/jcli-d-11-00716.1

Merlis, T. M., Schneider, T., Bordoni, S., & Eisenman, I. (2013b). Hadley circulation response to orbital precession. Part II: Subtropical continent. *Journal of Climate*, *26*(3), 754–771. https://doi.org/10.1175/jcli-d-12-00149.1

Merlis, T. M., Schneider, T., Bordoni, S., & Eisenman, I. (2013c). The tropical precipitation response to orbital precession. *Journal of Climate*, *26*(6), 2010–2021. https://doi.org/10.1175/jcli-d-12-00186.1

Myers, T. A., Scott, R. C., Zelinka, M. D., Klein, S. A., Norris, J. R., & Caldwell, P. M. (2021). Observational constraints on low cloud feedback reduce uncertainty of climate sensitivity. *Nature Climate Change*, *11*(6), 501–507. https://doi.org/10.1038/s41558-021-01039-0

Nadeau, A., & McGehee, R. (2017). A simple formula for a planet's mean annual insolation by latitude. *Icarus*, *291*, 46–50. https://doi.org/10.1016/j.icarus.2017.01.040

North, G. R. (1975). Analytical solution to a simple climate model with diffusive heat transport. *Journal of the Atmospheric Sciences*, *32*(7), 1301–1307. https://doi.org/10.1175/1520-0469(1975)032<1301:astasc>2.0.co;2

Persad, G. G., & Caldeira, K. (2018). Divergent global-scale temperature effects from identical aerosols emitted in different regions. *Nature Communications*, *9*(1), 3289. https://doi.org/10.1038/s41467-018-05838-6

Rose, B. E., Armour, K. C., Battisti, D. S., Feldl, N., & Koll, D. D. (2014). The dependence of transient climate sensitivity and radiative feedbacks on the spatial pattern of ocean heat uptake. *Geophysical Research Letters*, *41*(3), 1071–1078. https://doi.org/10.1002/2013gl058955

Rugenstein, M. A., Caldeira, K., & Knutti, R. (2016). Dependence of global radiative feedbacks on evolving patterns of surface heat fluxes. *Geophysical Research Letters*, *43*(18), 9877–9885. https://doi.org/10.1002/2016gl070907

Scott, R. C., Myers, T. A., Norris, J. R., Zelinka, M. D., Klein, S. A., Sun, M., & Doelling, D. R. (2020). Observed sensitivity of low-cloud radiative effects to meteorological perturbations over the global oceans. *Journal of Climate*, *33*(18), 7717–7734. https://doi.org/10.1175/jcli-d-19-1028.1

Smith, C. J., Kramer, R. J., & Sima, A. (2020). The HadGEM3-GA7. 1 radiative kernel: The importance of a well-resolved stratosphere. *Earth System Science Data*, *12*(3), 2157–2168. https://doi.org/10.5194/essd-12-2157-2020

Soden, B. J., & Held, I. M. (2006). An assessment of climate feedbacks in coupled ocean–atmosphere models. *Journal of Climate*, *19*(14), 3354–3360. https://doi.org/10.1175/jcli3799.1

Soden, B. J., Held, I. M., Colman, R., Shell, K. M., Kiehl, J. T., & Shields, C. A. (2008). Quantifying climate feedbacks using radiative kernels. *Journal of Climate*, *21*(14), 3504–3520. https://doi.org/10.1175/2007jcli2110.1

Stouffer, R. J. (2004). Time scales of climate response. *Journal of Climate*, *17*(1), 209–217. https://doi.org/10.1175/1520-0442(2004)017<0209:tsocr>2.0.co;2

Stuecker, M. F., Timmermann, A., Jin, F.-F., Proistosescu, C., Kang, S. M., Kim, D., et al. (2020). Strong remote control of future equatorial warming by off-equatorial forcing. *Nature Climate Change*, *10*(2), 124–129. https://doi.org/10.1038/s41558-019-0667-6

Tilmes, S., Richter, J. H., Mills, M. J., Kravitz, B., MacMartin, D. G., Vitt, F., et al. (2017). Sensitivity of aerosol distribution and climate response to stratospheric SO_2 injection locations. *Journal of Geophysical Research: Atmospheres*, *122*(23), 12591–512615. https://doi.org/10.1002/2017jd026888

Visioni, D., MacMartin, D. G., & Kravitz, B. (2021). Is turning down the sun a good proxy for stratospheric sulfate geoengineering? *Journal of Geophysical Research: Atmospheres*, *126*(5), e2020JD033952. https://doi.org/10.1029/2020jd033952

Weaver, A. J., Eby, M., Kienast, M., & Saenko, O. A. (2007). Response of the Atlantic meridional overturning circulation to increasing atmospheric CO_2: Sensitivity to mean climate state. *Geophysical Research Letters*, *34*(5), L05708. https://doi.org/10.1029/2006gl028756

Winton, M., Adcroft, A., Dunne, J., Held, I., Shevliakova, E., Zhao, M., et al. (2020). Climate sensitivity of GFDL's CM4. 0. *Journal of Advances in Modeling Earth Systems*, *12*(1), e2019MS001838. https://doi.org/10.1029/2019ms001838

Winton, M., Takahashi, K., & Held, I. M. (2010). Importance of ocean heat uptake efficacy to transient climate change. *Journal of Climate*, *23*(9), 2333–2344. https://doi.org/10.1175/2009jcli3139.1

Wood, R., & Bretherton, C. S. (2006). On the relationship between stratiform low cloud cover and lower-tropospheric stability. *Journal of Climate*, *19*(24), 6425–6432. https://doi.org/10.1175/jcli3988.1

Xiang, B., Xie, S.-P., Kang, S. M., & Kramer, R. J. (2023). An emerging Asian aerosol dipole pattern reshapes the Asian summer monsoon and exacerbates northern hemisphere warming. *Npj Climate and Atmospheric Science*, *6*(1), 77. https://doi.org/10.1038/s41612-023-00400-8

Xiang, B., Zhao, M., Ming, Y., Yu, W., & Kang, S. M. (2018). Contrasting impacts of radiative forcing in the Southern Ocean versus southern tropics on ITCZ position and energy transport in one GFDL climate model. *Journal of Climate*, *31*(14), 5609–5628. https://doi.org/10.1175/jcli-d-17-0566.1

Xie, S.-P., Deser, C., Vecchi, G. A., Ma, J., Teng, H., & Wittenberg, A. T. (2010). Global warming pattern formation: Sea surface temperature and rainfall. *Journal of Climate*, *23*(4), 966–986. https://doi.org/10.1175/2009jcli3329.1

Yang, W., Vecchi, G. A., Fueglistaler, S., Horowitz, L. W., Luet, D. J., Muñoz, Á. G., et al. (2019). Climate impacts from large volcanic eruptions in a high-resolution climate model: The importance of forcing structure. *Geophysical Research Letters*, *46*(13), 7690–7699. https://doi.org/10.1029/2019gl082367

Zhang, B., Zhao, M., & Tan, Z. (2023). Using a Green's function approach to diagnose the pattern effect in GFDL AM4 and CM4. *Journal of Climate*, *36*(4), 1105–1124. https://doi.org/10.1175/jcli-d-22-0024.1

Zhang, R., & Delworth, T. L. (2005). Simulated tropical response to a substantial weakening of the Atlantic thermohaline circulation. *Journal of Climate*, *18*(12), 1853–1860. https://doi.org/10.1175/jcli3460.1

Zhang, X., Deser, C., & Sun, L. (2021). Is there a tropical response to recent observed Southern Ocean cooling? *Geophysical Research Letters*, *48*(5), e2020GL091235. https://doi.org/10.1029/2020gl091235

Zhao, M. (2022). An investigation of the effective climate sensitivity in GFDL's new climate models CM4. 0 and SPEAR. *Journal of Climate*, *35*(17), 1–62. https://doi.org/10.1175/jcli-d-21-0327.1

Zhao, M., Golaz, J. C., Held, I., Guo, H., Balaji, V., Benson, R., et al. (2018a). The GFDL global atmosphere and land model AM4. 0/LM4. 0: 1. Simulation characteristics with prescribed SSTs. *Journal of Advances in Modeling Earth Systems*, *10*(3), 691–734. https://doi.org/10.1002/2017ms001208

Zhao, M., Golaz, J. C., Held, I., Guo, H., Balaji, V., Benson, R., et al. (2018b). The GFDL global atmosphere and land model AM4. 0/LM4. 0: 2. Model description, sensitivity studies, and tuning strategies. *Journal of Advances in Modeling Earth Systems*, *10*(3), 735–769. https://doi.org/10.1002/2017ms001209

Zhou, C., Zelinka, M. D., & Klein, S. A. (2017). Analyzing the dependence of global cloud feedback on the spatial pattern of sea surface temperature change with a Green's function approach. *Journal of Advances in Modeling Earth Systems*, *9*(5), 2174–2189. https://doi.org/10.1002/2017ms001096